INTERNATIONAL JOURNAL FOR NUMERICAL METHODS IN FLUIDS
Int. J. Numer. Meth. Fluids (2011)
Published online in Wiley Online Library (wileyonlinelibrary.com). DOI: 10.1002/fld.2713

A new enrichment space for the treatment of discontinuous pressures in multi-fluid flows

Roberto F. Ausas[1], Gustavo C. Buscaglia[1] and Sergio R. Idelsohn[2,*,†]

[1]*Instituto de Ciências Matemáticas e de Computação, Universidade de São Paulo, Av. do Trabalhador são–carlense 400, Centro, 13566-590, São Carlos, SP, Brazil*
[2]*ICREA Research Professor, Centro Internacional de Métodos Numéricos en Ingeniería., Edificio C1, Campus Norte UPC C/ Gran Capitán S/N 08034 Barcelona, Spain*

SUMMARY

In this work, a new enrichment space to accommodate jumps in the pressure field at immersed interfaces in finite element formulations, is proposed. The new enrichment adds two degrees of freedom per element that can be eliminated by means of static condensation. The new space is tested and compared with the classical P_1 space and to the space proposed by Ausas *et al* (Comp. Meth. Appl. Mech. Eng., Vol. 199, 1019–1031, 2010) in several problems involving jumps in the viscosity and/or the presence of singular forces at interfaces not conforming with the element edges. The combination of this enrichment space with another enrichment that accommodates discontinuities in the pressure gradient has also been explored, exhibiting excellent results in problems involving jumps in the density or the volume forces. Copyright © 2011 John Wiley & Sons, Ltd.

Received 16 May 2011; Revised 22 September 2011; Accepted 2 October 2011

KEY WORDS: multi-fluids; two-phase flows; embedded interfaces; finite element method; surface tension; discontinuous pressures; kinks

1. INTRODUCTION

The simultaneous presence of multiple fluids with varying properties in external or internal flows is found in daily life, marine environmental problems, and numerous industrial processes, among many other practical situations. Examples of these flows are gas–liquid transport, magma chambers, fluid-fuel interactions, crude oil recovery, spray cans, sediment transport in rivers and floods, pollutant transport in the atmosphere, cloud formation, fuel injection in engines, bubble column reactors and spray dryers for food processing, among others. This shows the importance of multi-fluid flows, which probably occur even more frequently than single phase flows [1]. As a result of the interaction between the different fluid components, multi-fluid flows are rather complex and very difficult to describe theoretically. For homogeneous flows, computational of fluid dynamics (CFD) has already a long history, and it is standard practice to use commercially available CFD codes. However, because of the complex physics involved in multi-fluid flows, the application of CFD in this area is rather young. Physical modeling in ad hoc laboratory scale models is not suitable for this purpose because of its complexity, the difficulty for scaling up to real life problems, and hence unaffordable costs. The alternative is, therefore, numerical modeling.

Despite the practical importance of the problem and the intensive work carried out in the last decade for the development of suitable mathematical and computational models, it is widely

*Correspondence to: Sergio R. Idelsohn, Centro Internacional de Métodos Numéricos en Ingeniería., Edificio C1, Campus Norte UPC C/ Gran Capitán S/N 08034 Barcelona, Spain.

†E-mail: sergio@cimne.upc.edu

accepted that the numerical study of heterogeneous flows is still a major challenge [1]. The complicated mathematical structure of the multi-fluid problem, multi-scale features of the flow, the existence of one or multiple internal interfaces and the unsteadiness of the flow, constitute major challenges for the analysis.

Computing the interface between various immiscible fluids or the free surfaces is difficult because neither the shape nor the positions of the interfaces are known a priori. The two approaches to solve these problems are: interface-tracking and interface-capturing methods. The former computes the motion of the flow particles via a Lagrangian approach where the computational domain adapts itself to the shape and position of the interfaces (see e.g., [2–7]). A different approach for the simulation of free-surface flows that is based on Lagrangian particles can be found in [8–11]. On the other hand, in the front-tracking method (see [12–14]), the interface is represented by a surface mesh advected with a Lagrangian method while immersed in an Eulerian (fix) mesh where the flow problem is solved considering the fluids as a single effective fluid with variable properties.

The other alternative is the interface-capturing method. Popular methods of this type are the volume-of-fluid technique (see [15–17]) and the level set method (see, for example, [18–21]). In this case, the flow problem is also solved in a fixed underlying mesh considering a single fluid with variable properties. Variants of these methods mainly differ in two aspects: First, the technique used to solve the transport equation for the scalar function where the interface is embedded, for which a great deal of work has been carried out to improve accuracy for purely Eulerian methods [22–27] and for semi-Lagrangian methods [28–30]. Second, the technique used to solve the Navier–Stokes equations for a one-phase flow with variable properties and in how the fluid-dynamical variables are treated near the interface because these can exhibit discontinuities in their values and/or their gradients owing to the discontinuities in the physical properties and/or the presence of singular forces.

Several remedies have been proposed to improve accuracy and robustness of computations in Eulerian formulations. For instance, in Brackbill *et al*. [31], a treatment of the singular forces at the interface by means of a regularization is proposed, such that sharp variations in the pressure field are avoided. In Löhner *et al*. [32] and Carrica *et al*. [33], different extrapolation techniques of the velocity and pressure near the interface are presented.

In this work, on the other hand, we focus the attention on how to improve the accuracy of simulations in finite element formulations by means of improving the approximation spaces. In this case, because a partition of the computational domain into simplices is made, and the interface does not necessarily conform to the element edges, standard finite element methods, either continuous or discontinuous across inter-element boundaries, suffer from suboptimal approximation orders. This poor approximation leads to spurious velocities near the interface that may significantly affect precision and robustness of numerical simulations (see e.g., [34]). One possibility is to locally modify the finite element spaces in those elements cut by the interface to accommodate the discontinuities. This can be carried out without introducing additional degrees of freedom, using the pressure space proposed by Ausas *et al*. [35]. The interpolation properties of this space are discussed in detail in [36], where the authors show that the interpolation order of this space is $\mathcal{O}(h^{\frac{3}{2}})$ in the $L^2(\Omega)$-norm, which represents an improvement with respect to the order $\mathcal{O}(h^{\frac{1}{2}})$ of the classical P_1-conforming space.

The other possibility that is explored in this article is to add degrees of freedom or enrich the finite element space at the elements cut by the interface. Minev *et al*. [37], and later Chessa and Belytschko [38], adopted an enrichment technique nowadays called XFEM, a name coined in the context of crack mechanics [39]. Both approaches lead to optimal orders of convergence, but the main drawback is that the additional degrees of freedom cannot be eliminated before assembly. The connectivity of the unknowns depend on the position of the interface, therefore, the mesh graph needs to be updated as the interface moves. Also, it has been observed that the resulting linear system becomes ill-conditioned because the linear independence of the finite element basis deteriorates as the mesh size is reduced. The XFEM approach has also been used recently in [40–42] for two-phase flows. A method that avoids the inclusion of additional degrees of freedom is the one presented by Fries *et al*. [43], which, on the other hand, has the drawback of the second-neighbor connectivity

DOI: 10.1002/fld

arising from the moving least square approach they use. Also, in [44], Codina and Coppola-Owen introduced an enrichment for the treatment of kinks in the pressure field as typically happens in problems with jumps in the density in the presence of a gravitational field. The additional degree of freedom can be statically condensed prior to assembly.

The main contribution of this paper is a new enrichment space for discontinuous pressures. Two enrichment functions are introduced at the elements crossed by the interface. The new functions are local to each element, linear on each side of the interface, discontinuous just at the interface and zero at the element nodes. The additional degrees of freedom can be condensed before assembly, avoiding the complexities associated with the update of the mesh graph. The implementation in any existing finite element code is extremely easy in two and three spatial dimensions, because the new shape functions are based on the usual P_1 functions. As illustrated in the numerical experiments, the interpolation properties of this new enrichment space are equal or better than those of the space presented in [35].

By way of outline, after this introduction, the governing equations and different jump conditions that arise in two-phase flows are recalled as well as the continuous and discrete variational formulations. Next, the new proposed enrichment space for discontinuous pressures is introduced with details to construct the enrichment functions. In Section 4, several problems in 2D and 3D are solved. Then, a further enrichment is proposed to deal with problems involving both discontinuities and kinks in the pressure field, in which, the new enrichment space is combined with the enrichment of [44]. Finally, some conclusions are drawn.

2. MATHEMATICAL SETTING

We restrict our attention here to problems governed by the incompressible Navier–Stokes equations. Let us consider a domain $\Omega \subset \mathbb{R}^d$ ($d = 2$ or 3). The problem is to find a velocity field $\mathbf{u}$ and a pressure field p such that

$$\rho\left(\partial_t \mathbf{u} + \mathbf{u}\cdot\nabla\mathbf{u}\right) - \nabla\cdot\left(2\,\mu\nabla^S\mathbf{u}\right) + \nabla p = \rho\,\boldsymbol{b} \quad \text{in } \Omega,\ t>0, \tag{1}$$

$$\nabla\cdot\mathbf{u} = 0 \quad \text{in } \Omega,\ t>0, \tag{2}$$

$$\mathbf{u} = \mathbf{u}_{\partial\Omega} \quad \text{in } \partial\Omega,\ t>0, \tag{3}$$

$$\mathbf{u} = \mathbf{u}_0 \quad \text{in } \Omega,\ t=0, \tag{4}$$

where $\mathbf{b}$ is a volume force, $\mathbf{u}_{\partial\Omega}$ are the Dirichlet boundary conditions and $\mathbf{u}_0$ is the initial condition for the velocity field. Although many phases can be present, we restrict here for the sake of simplicity to the case of two-phase flows. Denoting them by the plus '+' and minus '−' symbols, the fluid properties (density and viscosity) are given by

$$(\rho(\mathbf{x}),\mu(\mathbf{x})) = \begin{cases} (\rho^+,\mu^+) & \text{if } \mathbf{x}\in\Omega^+ \\ (\rho^-,\mu^-) & \text{if } \mathbf{x}\in\Omega^- \end{cases} \tag{5}$$

The fluid domains Ω^+ and Ω^- are separated by an interface denoted by Γ. In the following section, we comment on the boundary or jump conditions at this internal interface.

2.1. *Difficulties in the numerical solution of multi-phase flows-jump conditions*

In the numerical approximation of incompressible multi-fluid flows, several issues have to be considered:

1. a correct definition of the interface position;
2. possible pressure gradient jumps or kinks at the interface where density jumps are present;
3. possible pressure jumps at the interface where viscosity jumps are present;

DOI: 10.1002/fld

4. possible gradient velocity jumps where viscosity jumps are present; and
5. possible pressure jumps where surface tension is present.

Some of these aspects and possible numerical solutions have been previously discussed in [9] for Lagrangian formulations in which moving meshes are used. In this paper, we restrict our attention to items 2–5 of the preceding list for the case of Eulerian formulations in which fixed meshes are used instead. Let us now see how these jumps appear in the different cases mentioned.

Pressure gradient jumps
Density jumps introduce a kink in the pressure field at the interface. This can be easily seen in the example of two fluids with different densities at rest, one on top of the other inside a closed cavity. The hydrostatic pressure gradient is discontinuous at the interface. Because in this case, the solution corresponds to an identically zero velocity field, the pressure gradient is simply given by

$$\nabla p = \rho\,\mathbf{b},$$

if the density has a jump at the interface, and the volume force is continuous, we have

$$[\![\nabla p]\!] = [\![\rho\,\mathbf{b}]\!] = [\![\rho]\!]\,\mathbf{b} = (\rho^+ - \rho^-)\,\mathbf{b}, \tag{6}$$

where $[\![\cdot]\!]$ represents the jump of any quantity at the interface. A similar situation can occur in the case of a discontinuous volume force. This could be the case of an electric force acting just on one of the fluids, having for instance distributed electrical charges. As mentioned earlier, a remedy for this problem is the enrichment proposed in [44], which is later recalled.

Jump conditions for a Newtonian fluid
The standard jump conditions at internal boundaries are briefly recalled here. In the first place, the normal $\mathbf{n}$ to Γ is extended away from the interface by the closest-point projection; that is,

$$\mathbf{n}(\mathbf{x}) = \mathbf{n}(\pi_\Gamma(\mathbf{x})) \tag{7}$$

where

$$\pi_\Gamma(\mathbf{x}) = \arg\min_{\mathbf{y}\in\Gamma} \|\mathbf{x}-\mathbf{y}\| \tag{8}$$

This allows to decompose the velocity field $\mathbf{u}$ near the interface into its normal and tangential parts,

$$\mathbf{u} = u_n\mathbf{n} + \mathbf{u}_s, \tag{9}$$

where $u_n = \mathbf{u}\cdot\mathbf{n}$. The interface forces must balance the sum of the forces exerted on Γ from the 'positive' side, plus those from the 'negative' side. This is expressed as

$$(\sigma^- - \sigma^+)\cdot\mathbf{n} = \mathbf{f}_\Gamma. \tag{10}$$

Now, for the *normal component* of this jump, we have

$$[(\sigma^- - \sigma^+)\cdot\mathbf{n}]\cdot\mathbf{n} = [\![\sigma_{nn}]\!] = [\![-p + 2\,\mu\frac{\partial u_n}{\partial n}]\!] = f_{\Gamma n}. \tag{11}$$

For the tangential component, we project the right hand side of Equation (10) onto the tangent plane to the interface

$$\begin{aligned}\Pi_\Gamma\left[(\sigma^- - \sigma^+)\cdot\mathbf{n}\right] &= \left[\!\left[\mu\left(\frac{\partial\mathbf{u}_s}{\partial n} + \nabla_\Gamma u_n - \mathbb{H}\cdot\mathbf{u}_s\right)\right]\!\right] = \\ &= \left[\!\left[\mu\frac{\partial\mathbf{u}_s}{\partial n}\right]\!\right] + [\![\mu]\!](\nabla_\Gamma u_n - \mathbb{H}\cdot\mathbf{u}_s) = \mathbf{f}_{\Gamma s},\end{aligned} \tag{12}$$

where Π_Γ is the tangential projector operator, that for a given vector $\mathbf{w}$ is given by

$$\Pi_\Gamma\mathbf{w} = \mathbf{w}_s = \mathbf{w} - w_n\mathbf{n} = (\mathbb{I} - \mathbf{n}\otimes\mathbf{n})\,\mathbf{w}, \tag{13}$$

DOI: 10.1002/fld

The symbol ∇_Γ is the surface gradient, which, for a function f defined on Γ, is given by

$$\nabla_\Gamma f = \Pi_\Gamma \nabla \tilde{f}, \tag{14}$$

where $\tilde{f} \in \mathcal{C}^1$ is any extension out of Γ of f. Finally, $\mathbb{H}$ $(= \nabla_s \mathbf{n})$ is a symmetric tensor called the second fundamental form. This tensor contains the geometrical information of the interface. In particular, its trace is the well known mean curvature κ. For a quick review of these formulae from differential geometry in the context of capillary flows, the reader is referred to the recent article by Buscaglia and Ausas [45].

Remark: In the general case, both the pressure and the velocity gradient can be discontinuous at the interface. However, for problems involving surface tension, in the absence of Marangoni or thermocapillary effects, the force $\mathbf{f}_\Gamma$ is normal to the interface and given by

$$\mathbf{f}_\Gamma = \gamma \kappa \mathbf{n}, \tag{15}$$

where γ is the (constant) surface tension coefficient. If viscosities of both fluids are the same, just the pressure exhibits a jump. In the numerical solution of problem (1)–(4) with jump conditions (6), (11) and (12), regardless of the method used (finite elements, finite differences, etc.), special care has to be taken to accommodate the discontinuities in the fluid-dynamical variables near the interface. In this article, we use a finite element method of which the variational formulation is presented succeedingly. In this case, the key issue relies on how to choose the approximation spaces for pressure and velocity.

2.2. Variational formulation

The variational formulation for the problem to be solved is

Find $(\mathbf{u}, p) \in V \times Q$ *such that*

$$\begin{aligned} \int_\Omega \rho\,(\partial_t \mathbf{u} + \mathbf{u}\cdot\nabla\mathbf{u})\cdot\mathbf{v}\,\mathrm{d}\Omega + \int_\Omega 2\mu\, D\mathbf{u} : D\mathbf{v}\,\mathrm{d}\Omega - \\ - \int_\Omega p\,\nabla\cdot\mathbf{v}\,\mathrm{d}\Omega = \int_\Omega \mathbf{b}\cdot\mathbf{v}\,\mathrm{d}\Omega + \mathbf{f}_\Gamma(\mathbf{v}) \end{aligned} \tag{16}$$

$$\int_\Omega q\,\nabla\cdot\mathbf{u}\,\mathrm{d}\Omega = 0 \tag{17}$$

$\forall (\mathbf{v}, q) \in V \times Q$. The term $\mathbf{f}_\Gamma(\mathbf{v})$ in Equation (16) represents the contribution of a singular force concentrated at the interface Γ. For the case of surface tension, we use a Laplace–Beltrami formulation (see e.g., [34, 40, 45, 46]), that is,

$$\mathbf{f}_\Gamma(\mathbf{v}) = -\int_\Gamma \gamma(\mathbf{x})\,(\mathbb{I} - \mathbf{n}\otimes\mathbf{n}) : \nabla\mathbf{v}\,d\Gamma, \tag{18}$$

that accounts for both,surface tension and Marangoni effects.

We use a stabilized formulation based on the ASGS (Algebraic Subgrid Scale) method for discretization (see, e.g., [47] and references therein) together with a trapezoidal rule for temporal discretization and a monolithic approach solving simultaneously for velocity and pressure using a Newton–Raphson iterative method. The discrete variational formulation of this problem then reads

Find $(\mathbf{u}_h^{n+1}, p_h^{n+1}) \in V_h \times Q_h$ *such that*

$$\begin{aligned} \mathcal{R}_\mathbf{u} = \int_\Omega \mathcal{G}_\mathbf{u}\cdot\mathbf{v}_h\,\mathrm{d}\Omega + \int_\Omega 2\mu\nabla^S\mathbf{u}_h^{n+1} : \nabla\mathbf{v}_h\,\mathrm{d}\Omega - \int_\Omega p_h^{n+1}\nabla\cdot\mathbf{v}_h\,\mathrm{d}\Omega + \mathbf{f}_{\Gamma_h}^{n+1}(\mathbf{v}_h) + \\ + \sum_{K\in\mathcal{T}_h}\tau_K\int_{\Omega_K}(\mathcal{G}_\mathbf{u} + \nabla p_h^{n+1})\cdot\mathbf{u}_h^n\cdot\nabla\mathbf{v}_h + \sum_{K\in\mathcal{T}_h}\int_{\Omega_K}\delta_K\,\nabla\cdot\mathbf{u}_h^{n+1}\,\nabla\cdot\mathbf{v}_h\,\mathrm{d}\Omega = 0 \end{aligned} \tag{19}$$

$$\mathcal{R}_p = \int_\Omega q_h\,\nabla\cdot\mathbf{u}_h^{n+1}\,\mathrm{d}\Omega + \sum_{K\in\mathcal{T}_h}\int_{\Omega_K}\frac{\tau_K}{\rho}(\mathcal{G}_\mathbf{u} + \nabla p_h^{n+1})\cdot\nabla q_h\,\mathrm{d}\Omega = 0 \tag{20}$$

DOI: 10.1002/fld

$\forall(\mathbf{v}_h, q_h) \in V_h \times Q_h$. In (19), the term $\boldsymbol{\mathcal{G}_u}$ is given by

$$\boldsymbol{\mathcal{G}}_{\mathbf{u}} = \rho \left(\frac{\mathbf{u}_h^{n+1} - \mathbf{u}_h^n}{\Delta t} + \mathbf{u}_h^{n+1} \cdot \nabla \mathbf{u}_h^{n+1} - \boldsymbol{b}^{n+1} \right), \tag{21}$$

with Δt the time step and the stabilization parameters given by

$$\tau_K = c \left[4\frac{\nu}{h^2} + 2\frac{|\mathbf{u}_h|_\infty^n}{h} \right]^{-1}, \quad \delta_K = 2\,\mu + \rho\,|\mathbf{u}_h|_\infty^n\,h_K, \tag{22}$$

where c is a tuning parameter, that for the academic problems shown in Section 4 is taken equal to 1, whereas for the 3D examples, is taken equal to 0.1.

Many authors introduce a regularized form of the Dirac delta function for the computation of $\mathbf{f}_{\Gamma_h}^{n+1}(\mathbf{v}_h)$ in (19) as proposed in [31, 48], therefore, the surface force is approximated as a volume force more or less concentrated around Γ depending on an adjustable regularization parameter. In our formulation, we *do not* use such regularizations and instead compute this term exactly, which precisely leads to sharp variations through the interface in the pressure field. Solving problem (19)–(20) accuratelly, requires the finite element spaces to be appropriately chosen, so as to accomodate discontinuities and/or kinks in the pressure and velocity fields. We first focus on how to improve the accuracy of the numerical approximation in several problems involving jumps in the pressure field, for which we introduce a *new* enrichment space.

3. NEW ENRICHMENT SPACE FOR DISCONTINUOUS PRESSURES

First, consider a finite element partition $\mathcal{T}_h$ of the domain Ω into simplices (triangles in the 2D case and tetrahedra in the 3D case) and denote each element in the partition as Ω_K. The number of vertices per element is denoted by n_p (equal to three for triangles and four for tetrahedra). The interface Γ_h is composed of straight segments (in 2D) or planar facets (in 3D) and does not conform to the element edges. The element Ω_K can then be split into two subelements Ω_K^+ and Ω_K^-. We illustrate a typical element cut by Γ_h in two and three spatial dimensions and the corresponding subdomains in Figure 1. Those cases in which the interface passes through the nodes are degenerate cases that are not considered here. As noticed in Figure 1 for the 3D case, two possible situations have to be considered, because the reconstructed interface can be either a triangular or a quadrangular facet. In the discrete variational formulation presented earlier, the integrals over the elements are performed exactly just by redefining the quadrature rule in the elements cut by the interface after subdivision following Γ_h. The velocity field is made up of continuous linear functions. For all the elements of $\mathcal{T}_h$ that are not crossed by Γ_h, the space Q_h is also made up of continuous linear functions. *The various possibilities to improve accuracy of the numerical approximation in problems involving jumps or kinks, consist in an enrichment or a modification of the finite element space Q_h only in those elements of $\mathcal{T}_h$ crossed by Γ_h.*

The discrete pressure proposed here can be written as

$$p_h = \sum_{J \in \mathcal{J}} P_J\, N_J + \sum_{J \in \mathcal{J}_e} C_J\, M_J, \tag{23}$$

where $\mathcal{J} = \{1, \ldots, n_P\}$, with n_P the number of standard degrees of freedom per element and $\mathcal{J}_e$ the set of indices accounting for the additional enrichment functions local to the element.

To build the new pressure space, a requirement for the enrichment is that a constant solution on each fluid domain with a jump at the interface belong to the discrete space Q_h. To satisfy this requirement, we introduce two new enrichment functions that are linear on each subelement Ω_K^+ and Ω_K^- and discontinuous at Γ_h. We also require both functions to be zero at the nodes of the simplex. By inspection, we see that a possibility to define the enrichment functions is as follows:

$$M_1(\mathbf{x}) = (1 - S(\mathbf{x}))\,\chi^+(\mathbf{x}), \tag{24}$$

$$M_2(\mathbf{x}) = S(\mathbf{x})\,\chi^-(\mathbf{x}), \tag{25}$$

DOI: 10.1002/fld

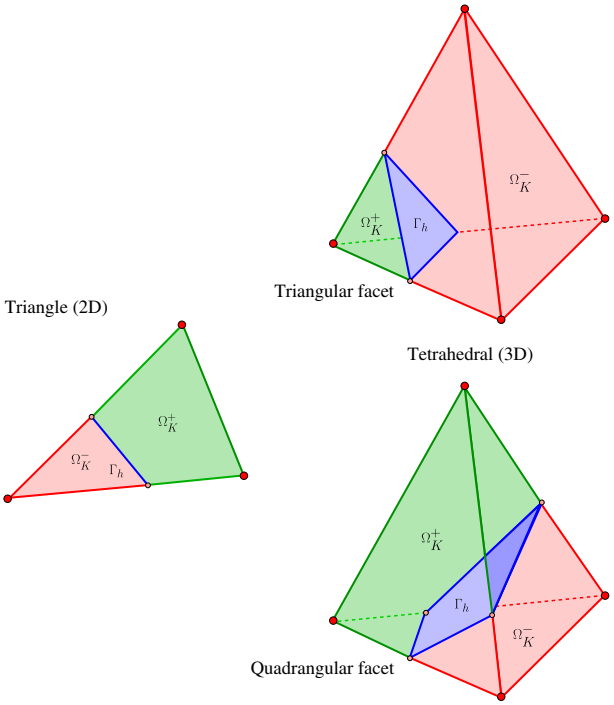

Figure 1. Typical element Ω_K, subelements Ω_K^+ and Ω_K^- and interface Γ_h.

where the function S is given in terms of the usual P_1 functions by

$$S = \sum_{J \in \mathcal{J}^+} N_J(\mathbf{x}), \tag{26}$$

with $\mathcal{J}^+ = \{J \in \mathcal{J}, \mathbf{x}_J \in \Omega_K^+\}$, and χ^+ and χ^- the characteristic functions for the positive and negative sides. The dimension of the pressure space is thus dim $Q_h = N_P + 2\,N_E$, where N_P and N_E are the total number of nodes and elements respectively in $\mathcal{T}_h$. However, because the additional shape functions are local to each element crossed by the interface, they can be condensed prior to assembly, and the size of the final linear system to be solved is the same as in the standard case. Note that this elimination can be carried out because the pressure is just involved in linear terms of the problem.

In Figure 2, the enrichment functions for a typical triangular element are shown. In the left part of the figure, the two functions are shown separately, and in the right part, they are plotted together just for illustrative purposes. In Table I, the computation of these functions is given in the form of a pseudo-code.

3.1. Static elimination of the enrichment unknowns

Before final assembly, the linear system to be solved at each non-linear iteration can be written by blocks as follows

$$\begin{bmatrix} \mathsf{A}_{SS} & \mathsf{A}_{SM} \\ \mathsf{A}_{MS} & \mathsf{A}_{MM} \end{bmatrix} \begin{bmatrix} \delta\mathbf{X}_S \\ \mathbf{X}_M \end{bmatrix} = - \begin{bmatrix} \mathcal{R}_S \\ \mathcal{F}_M \end{bmatrix} \tag{27}$$

where the subindex S refers to the velocity and standard pressure degrees of freedom and the subindex M refers to the additional degrees of freedom. At the elementary level the dimension

DOI: 10.1002/fld

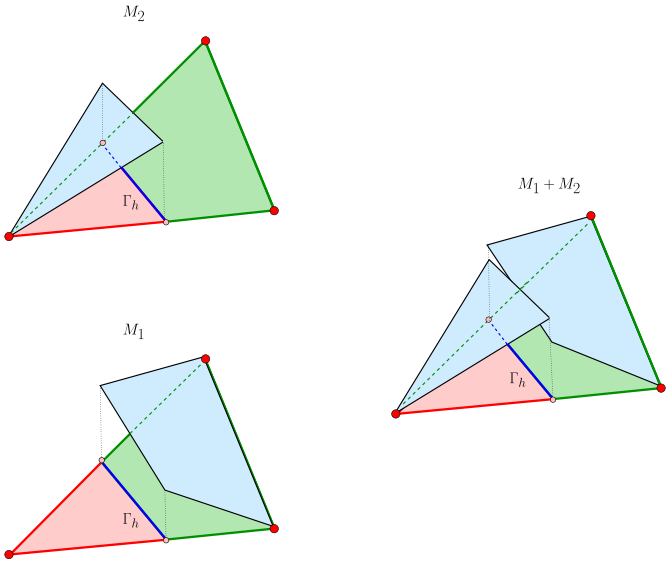

Figure 2. New enrichment functions in a typical triangular element. On the left, the two functions are drawn separately. On the right, the two functions are drawn together just for illustrative purposes.

Table I. Computation of the new enrichment functions. Nomenclature: n_p is the number of nodes per element, n_G is the number of integration points per subelement, N_J is the usual Jth linear basis function, M_I ($I = 1, 2$) are the new enrichment functions and X_J^K are the vertices coordinates of element Ω_K.

```
1: Subdivide element K in n_S subelements
2: do (s = 1, n_S)
3:  Set Gauss points x_j^s , for j = 1, ..., n_G
4:   do (i = 1, n_G)
5:    Set S(x_i^s) = 0
6:    do (J = 1, n_p)
7:     if (X_J^K ∈ Ω_K^+)
8:      Set S(x_i^s) ← S(x_i^s) + N_J(x_i^s)
9:    end if
10:  end do
11:  if (x_i^s ∈ Ω_K^+)
12:     Set M_1(x_i^s) = 1 − S(x_i^s)
13:     Set M_2(x_i^s) = 0
14:  else
15:     Set M_1(x_i^s) = 0
16:     Set M_2(x_i^s) = S(x_i^s)
17:  end if
18:  end do
19: end do
```

of matrix A_{SS} is $n_p^2 \times n_p^2$, of matrix A_{SM} is $n_p^2 \times 2$, of matrix A_{MS} is $2 \times n_p^2$ and of matrix A_{MM} is 2×2 and its IJ entry is given by

$$\mathsf{A}_{MM}^{IJ} = \frac{\tau_K}{\rho} \int_{\Omega_K} \nabla M_I \cdot \nabla M_J \, \mathrm{d}\Omega \tag{28}$$

DOI: 10.1002/fld

which for our case is a positive definite diagonal matrix because note that $M_1 = 0$ and $M_2 \neq 0$ in Ω_K^- and $M_1 \neq 0$ and $M_2 = 0$ in Ω_K^+. For the additional degrees of freedom, we do not compute the incremental values, but the unknown $\mathbf{X}_M$ because the pressure is just involved in the linear terms of the problem. Now, using the fact that the enrichment functions are local to each element, we eliminate $\mathbf{X}_M$ at the elementary level before final assembly as follows

$$\left[\mathsf{A}_{SS} - \mathsf{A}_{SM}(\mathsf{A}_{MM})^{-1}\mathsf{A}_{MS}\right]\delta\mathbf{X}_S = -\boldsymbol{\mathcal{R}}_S + \mathsf{A}_{SM}(\mathsf{A}_{MM})^{-1}\boldsymbol{\mathcal{F}}_M \tag{29}$$

The enrichment shape functions can be normalized to avoid round-off errors in the computation of $(\mathsf{A}_{MM})^{-1}$. The normalization factor can be defined simply by doing an order of magnitude estimation. Because, each entry of A_{MM} is the product of derivatives of two linear shape functions of order $\sim 1/h^2$ that are integrated over the element volume, which is of order $\sim h^d$ and the stabilization $\tau_K/\rho \sim h^2/\mu$ (considering the viscous dominated case for simplicity), the normalization factor can be chosen to be of order h^d/μ so as to end up with entries of order 1 in matrix A_{MM}.

Numerical results using the new enrichment space will be compared with the classical P_1-conforming space and with the space presented in [35], which is recalled here for completeness.

3.2. *Space of* [35] *for discontinuous pressures without additional unknowns*

The interpolation properties of the space proposed in [35] have also been discussed in [36]. In this space, no additional degrees of freedom are incorporated but the pressure shape functions are modified so as to capture discontinuities in the pressure field. The modifications are local and can be computed element-by-element. The modified functions are piecewise linear on each side and only discontinuous at the interface Γ_h. They form a nodal basis, in the sense that they take the value one at their corresponding node and zero at the other nodes. To define them, we simply 'carry' the value at each node towards the intersection of any edge emanating from it with the interface. The shape functions for a typical triangular element are shown in Figure 3, but again, the functions for the case of tetrahedral elements can be easily built as shown in the pseudo-code given in Table II.

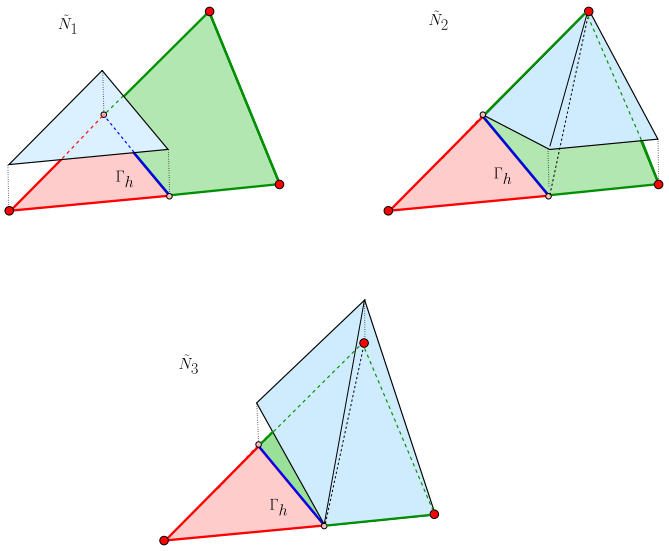

Figure 3. Finite element basis shape functions for the space proposed in [35] in a typical triangular element.

DOI: 10.1002/fld

Table II. Computation of the basis functions for the space of [35]. Nomenclature: n_p is the number of nodes per element, n_G is the number of integration points per subelement, N_J is the usual Jth linear basis function, $\tilde{N}_I$ ($I = 1, 2, 3$) are the modified basis functions and $\boldsymbol{X}_I^K$ are the vertices coordinates of element Ω_K.

```
1: Subdivide element K in n_S subelements
2: do (s = 1, n_S)
3:  Set subelement vertices X_J for J = 1, ..., n_p
4:  Set Gauss points x_j^s , for j = 1, ..., n_G
5:  do (i = 1, n_G)
6:   Set Ñ_I(x_i^s) = 0 for I = 1, ..., n_p
7:   do (I = 1, n_p)
8:    if ((X_I^K, x_i^s) ∈ Ω_K^+) || (X_I^K, x_i^s) ∈ Ω_K^-))
9:      do (J = 1, n_p)
10:       if (N_I(X_J^s) > 0) then
11:         Set Ñ_I(x_i^s) ← Ñ_I(x_i^s) + N_J(x_i^s)
12:       end if
13:     end do
14:   end if
15: end do
16: end do
```

4. NUMERICAL TESTS

4.1. Couette flow: Discontinuity in the pressure field because of a singular force

In the first experiment, we consider the domain $[0, L] \times [0, H]$, with periodic boundary conditions in the x_1-direction. The velocity is set to zero at the top and bottom boundaries

$$\mathbf{u}(x_1, x_2 = 0) = \mathbf{u}(x_1, x_2 = H) = 0$$

and the interface Γ is the straight vertical line $x_1 = a$, on which a constant unit normal force $f = 1$ is imposed. The exact solution for this problem is

$$u_1(x_1, x_2) = \frac{1}{2\mu L} x_2 (H - x_2) \tag{30}$$

$$u_2(x_1, x_2) = 0 \tag{31}$$

$$p(x_1, x_2) = -\frac{1}{L} x_1 + \mathcal{H}(x_1 - a) \tag{32}$$

The indeterminacy of the pressure is removed by imposing $p(0, 0) = 0$ instead of setting the average to zero, for simplicity. This problem, with $L = 3$, $H = 1$, $\mu = 1$ and $a = 2$ was discretized with the stabilized equal-order formulation presented earlier with the classical P_1-conforming pressure space, the space of [35] and the new enrichment space.

A sequence of unstructured meshes was built, of which the first one is shown in Figure 4. To this mesh, which consists of 3520 triangles, we assign a mesh size of $h = 0.044$. The following meshes in the sequence are built by subdivision. We measure the velocity error in the $H^1(\Omega)$-norm and the pressure error in the $L^2(\Omega)$-norm as functions of h for all three pressure spaces. The results of the convergence analysis are displayed in Figures 5 and 6. As seen in the figures, the error is very similar for both discontinuous spaces. The pressure field corresponding to the classical P_1-conforming pressure is compared with that obtained using the new enrichment space in Figure 7.

DOI: 10.1002/fld

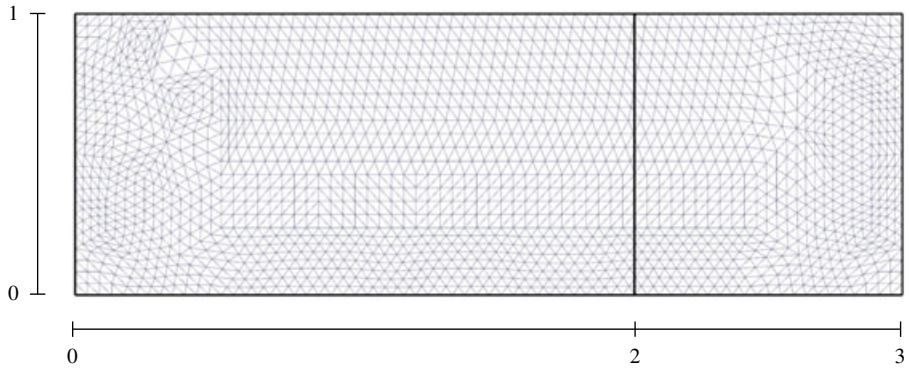

Figure 4. Mesh for the Couette flow problem convergence study, with 3520 elements and $h = 0.044$.

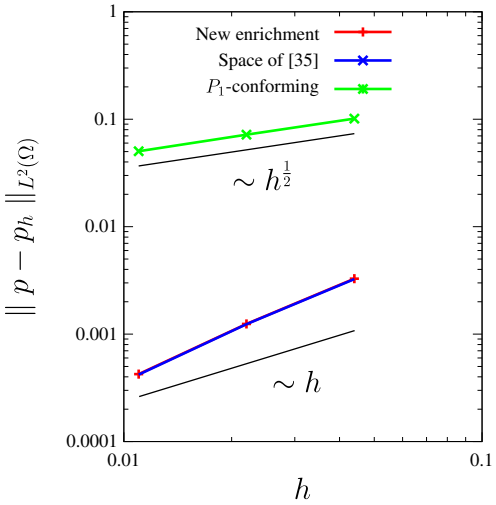

Figure 5. Error norm for the pressure field, showing the convergence rates for the Couette flow problem.

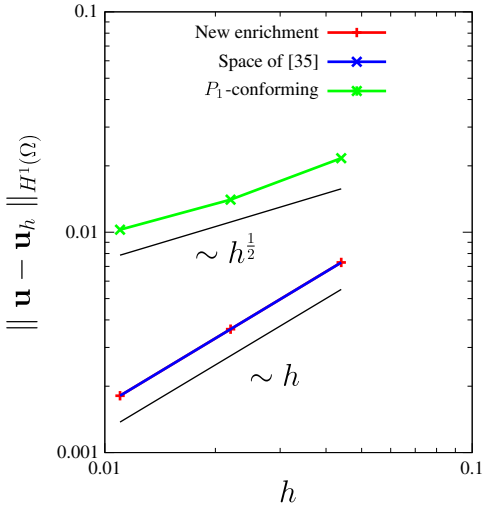

Figure 6. Error norm for the velocity field, showing the convergence rates for the Couette flow problem.

DOI: 10.1002/fld

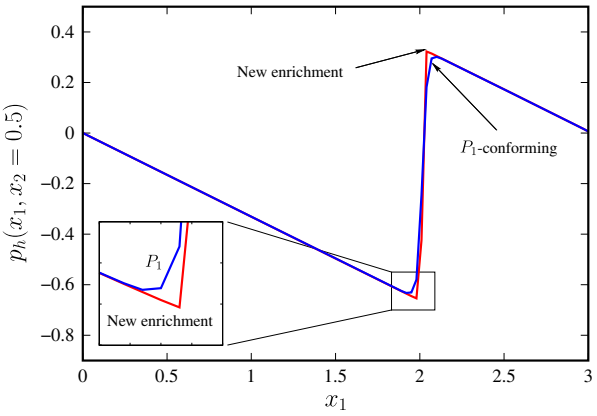

Figure 7. Pressure field section at $y = 0.5$ for the Couette flow problem.

From the figure, we see that the new enrichment space exhibits significantly better behavior near the interface than the classical P_1-conforming space. Results obtained using the space of [35] are similar to those corresponding to the new space.

4.2. *Extensional flow: discontinuity in the pressure field because of a jump in the viscosity*

We consider an extensional flow problem in which the computational domain $[0, 1] \times [0, 1]$ is split by an interface separating fluids with different viscosities μ_1 and μ_2. The density ρ is assumed the same for both fluids. In this case, the interface Γ is the straight horizontal line $x_2 = a$. Considering the following linear velocity field

$$u_1(x_1, x_2) = 1 - x_1, \tag{33}$$

$$u_2(x_1, x_2) = x_2, \tag{34}$$

and neglecting the volume forces, it can be easily found that the exact solution for the pressure field is quadratic on each fluid and with a jump at the interface because of the viscosity difference. This pressure field is given by

$$p(x_1, x_2) = \rho \left(x_1 - \tfrac{1}{2}(x_1^2 + x_2^2)\right) + 2(\mu_1 - \mu_2)\mathcal{H}(a - x_2) \tag{35}$$

where $\mathcal{H}(a-x_2) = 1$ if $x_2 < a$ and zero otherwise. The indeterminacy of the pressure in the simulations is again removed by imposing $p(1, 1) = 0$ instead of setting the average to zero. To reproduce this exact solution, the velocity field given by Equations (33)–(34) is imposed at the boundaries.

The problem is solved with $\rho = 10$, $\mu_1 = 5$ and $\mu_2 = 1$ and $a = 0.5$ using the classical P_1-conforming pressure space, the new enrichment space and the space of [35]. A sequence of unstructured meshes was built, of which the first one is shown in Figure 8. To this mesh, which consists of 832 triangles, we assign a mesh size of $h = 0.055$. The following meshes in the sequence are built by subdivision of each triangle into four equal triangles. We measure the velocity error in the $H^1(\Omega)$-norm and the pressure error in the $L^2(\Omega)$-norm as function of h. The results of the convergence analysis are displayed in Figures 9 and 10. Results for the new enrichment space exhibit, in this case a much smaller error (more than one order of magnitude) than results for the space of [35], in both pressure and velocity. Also, for the meshes considered, we observe a better convergence order of the new enrichment space, equal to h^2 for pressure and $h^{\frac{5}{2}}$ for velocity.

In Figure 11, the pressure field for the the new enrichment space (left) and the classical P_1-conforming pressure space (right) are shown. In Figure 12, cuts of these pressure fields at $x_1 = 0.5$ are compared, from which we clearly appreciate the better behavior near the interface when the new enrichment space is used. Note that the case without inertial effects (i.e., $\rho = 0$) corresponds to a constant pressure field on each fluid, with a jump at the interface of magnitude $2(\mu_1 - \mu_2)$. This

DOI: 10.1002/fld

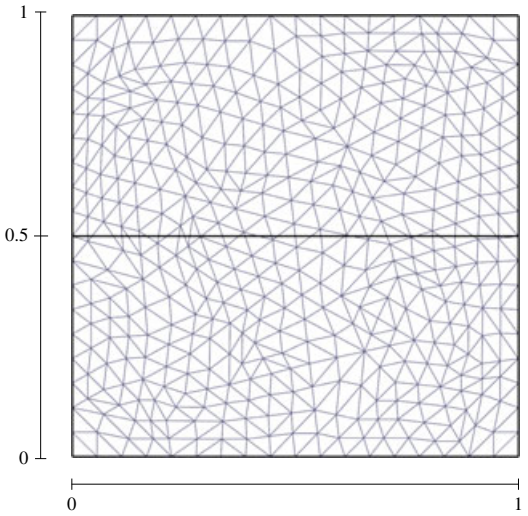

Figure 8. Mesh for the extensional flow problem convergence study, with 832 elements and $h = 0.055$.

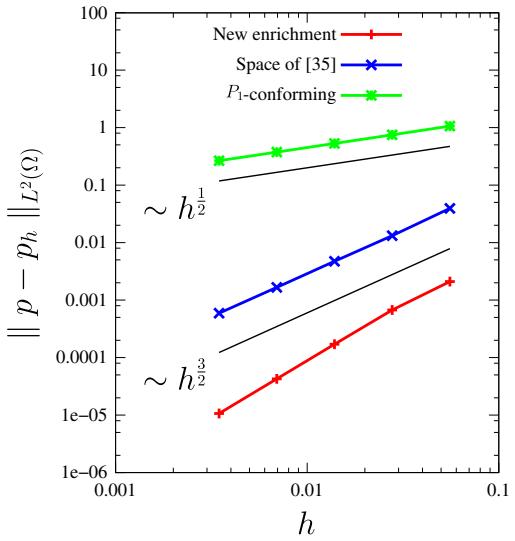

Figure 9. Error norm for the pressure field, showing the convergence rates for the extensional flow problem.

solution belongs to the finite element spaces when either, the new enrichment space or the space of [35] are used.

5. PROBLEMS WITH SURFACE TENSION

In the previous academic examples, the interface Γ was fixed. Now, we aim to illustrate the use of the new enrichment space in a more complex situation. In this article, a level set formulation is used, in which the interface is the zero set of a continuous scalar function ϕ, i.e.

$$\Gamma = \{\mathbf{x} \in \Omega,\ \phi(\mathbf{x}) = 0\}. \tag{36}$$

The level set function is transported according to the following hyperbolic equation

$$\partial_t \phi + \mathbf{u} \cdot \nabla \phi = 0. \tag{37}$$

DOI: 10.1002/fld

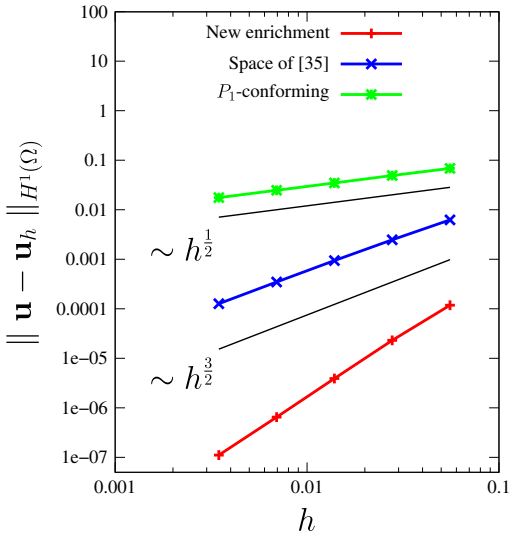

Figure 10. Error norm for the velocity, showing the convergence rates for the extensional flow problem.

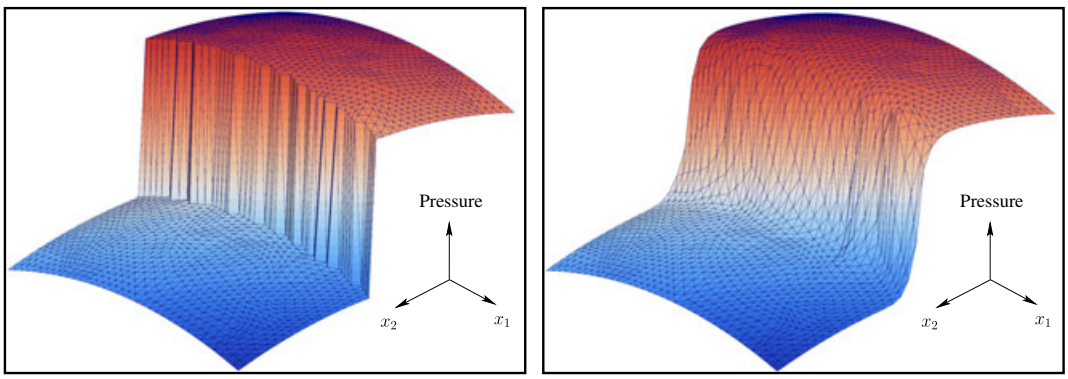

(a) New enrichment space

(b) P_1-conforming space

Figure 11. Pressure fields for the extensional flow problem. (a) New enrichment space. (b) P_1-conforming space.

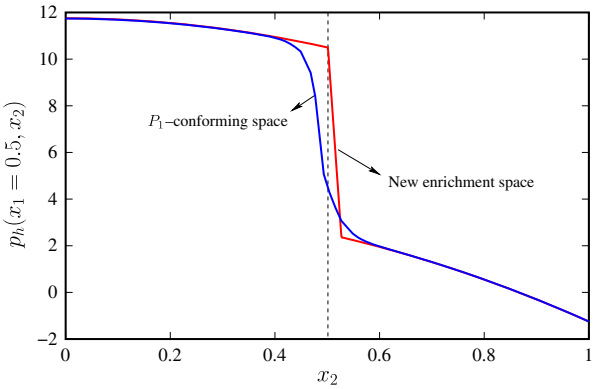

Figure 12. Comparison of the pressure field section at $x_1 = 0.5$ for the extensional flow problem using the new enrichment space and the P_1-conforming space.

DOI: 10.1002/fld

In the discrete case, the transport equation is solved simultaneously with the velocity and pressure fields by means of an SUPG (streamline-upwind-Petrov–Galerkin) method (see [49]), by adding the following problem to the variational formulation in Equations (19)–(20)

Find $\phi_h^{n+1} \in W_h$ *such that*

$$\sum_{K\in\mathcal{T}_h}\int_{\Omega_K}\left(\frac{\phi_h^{n+1}-\phi_h^n}{\Delta t}+\mathbf{u}_h^{n+1}\cdot\nabla\phi_h^{n+1}\right)\left(w_h+\tilde{\tau}_K\mathbf{u}_h^{n+1}\cdot\nabla w_h\right)\mathrm{d}\Omega=0 \tag{38}$$

$\forall w_h \times W_h$. The discrete space W_h is made up of continuous linear functions. The stabilization parameter $\tilde{\tau}_K$ is given by

$$\tilde{\tau}_K=\frac{\tilde{c}\,h}{2\,|\mathbf{u}_h|_\infty}, \tag{39}$$

where the factor $\tilde{c}$ is taken equal to 0.1.

With this formulation, we study the rise of a buoyant bubble. This problem has been solved many times before (see e.g., [50] and references therein). We assume a bubble with density $\rho_1 = 10^{-3}$ and viscosity μ_1 in a quiescent liquid with density $\rho_2 = 1$ and viscosity μ_2 in the computational domain $\Omega = (0, 2.25) \times (0, 2.25) \times (0, 4)$. At the initial time, the diameter D of the bubble is 1 and is placed at the position (1.125,1.125,1). The gravity $\mathbf{g}$ is taken equal to $-10\,\hat{e}_2$.

The Morton and Weber numbers are used to characterize the bubble's behavior and are defined as

$$\mathrm{Mo}=\frac{\|\mathbf{g}\|\,\mu_2^4}{\rho_2\,\gamma^3},\quad \mathrm{We}=\frac{\rho_2\,\|\mathbf{g}\|\,D^2}{\gamma} \tag{40}$$

The different regimes and shapes adopted by the bubbles can be identified in the well-known Grace's diagram [51]. We consider in this paper two different regimes corresponding to the following physical parameters

- Spherical regime: $\mu_1 = 3\times10^{-4}$, $\mu_2 = 0.3$, $\gamma = 10 \Rightarrow \mathrm{Mo} = 8.1\times10^{-5}$, $\mathrm{We} = 1$
- Skirted regime: $\mu_1 = 10^{-3}$, $\mu_2 = 0.1$, $\gamma = 0.1 \Rightarrow \mathrm{Mo} = 1$, $\mathrm{We} = 100$

In the first case, labeled spherical regime, the problem is dominated by surface tension effects and the bubble's shape remains approximately spherical during its evolution. In the second case, labeled skirted regime, surface tension effects are less important, and the bubble suffers a larger deformation during the evolution.

The discrete variational formulation with the new enrichment space was included into a general purpose in-house code, which is described elsewhere (see [52]). The level set function is periodically reinitialized by means of a mass-preserving redistancing scheme (see [53, 54]) to keep its distortion under control. For this problem, the finite element mesh used consists of $1,511,016$ tetrahedra, and the time step is taken equal to 5×10^{-4} for both regimes.

For the spherical regime, plotted in Figure 13 are the interface shapes at times $t = 0$, 0.375 and 0.75. The interface is painted with the velocity magnitude. The better mass conservation of the new enrichment space as compared with the classical P_1-conforming space are evident. In the former case, a 2% of the bubble's mass is lost at the final time, against a 60% in the case without enrichment.

For the skirted regime, to better appreciate the benefits of the new enrichment space, we plot in Figure 14 the bubbles at different times. We observe the typical cap shape attained by the bubble. For the case using the new enrichment, the bubble is plotted on the left, in red, whereas for the case using the classical P_1-conforming space, the bubble is plotted on the right, in blue. The mass loss is 0.14% in the first case and 15% in the second one, clearly evidencing the benefits of the new pressure space. For both regimes, similar results to those corresponding to the new enrichment are obtained if the space of [35] is used instead.

Finally, in Figure 15, we plot the position of the bubble's center of mass as a function of time. In this figure, we notice that after an initial transient the center of mass reaches an approximately constant velocity. With these velocities, a Reynolds number can be computed and compared with

DOI: 10.1002/fld

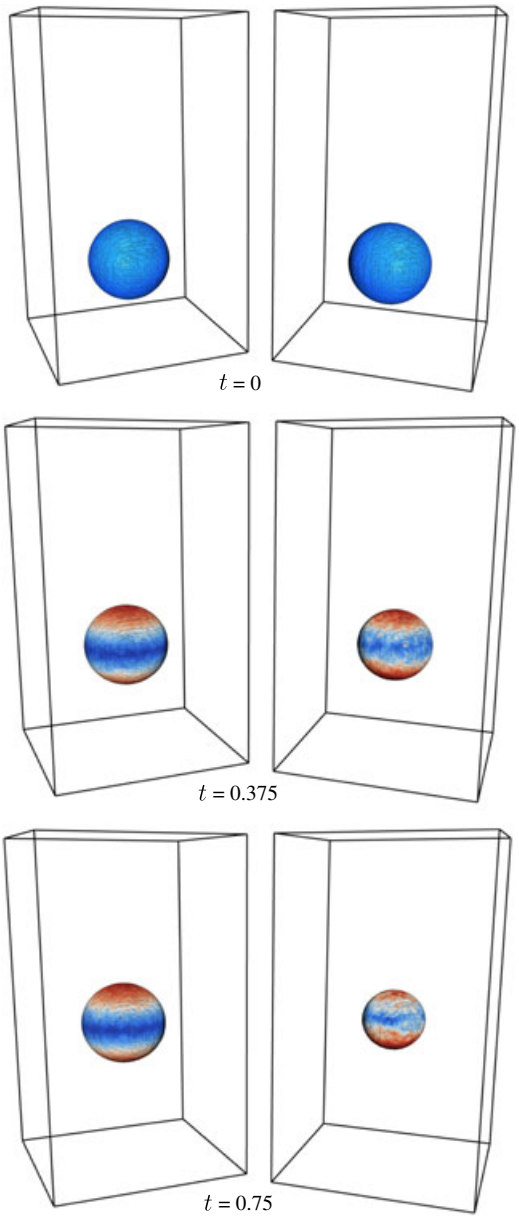

Figure 13. Comparison of the three-dimensional rising bubble at different times for the spherical regime, using the new enrichment space (left) and the classical P_1-conforming space (right). For times 0.375 and 0.75, the maximum of the color scale corresponds to 1.3 (red) and the minimum to 0.02 (blue).

the values reported in Grace's diagram [51] as performed by other authors (see e.g., [50]). In Table III, we present the Reynolds number Re_e obtained from Grace's diagram and the computed one Re_c obtained by performing a linear regression of the data shown in Figure 15 starting from time $t = 0.4$. Results presented in Table III show a difference of about 20% between experimental and numerical results.

6. FURTHER ENRICHMENTS

We now discuss two further enrichments to improve accuracy of the numerical approximation in problems involving discontinuities and/or kinks. On the one hand, we combine the enrichment

DOI: 10.1002/fld

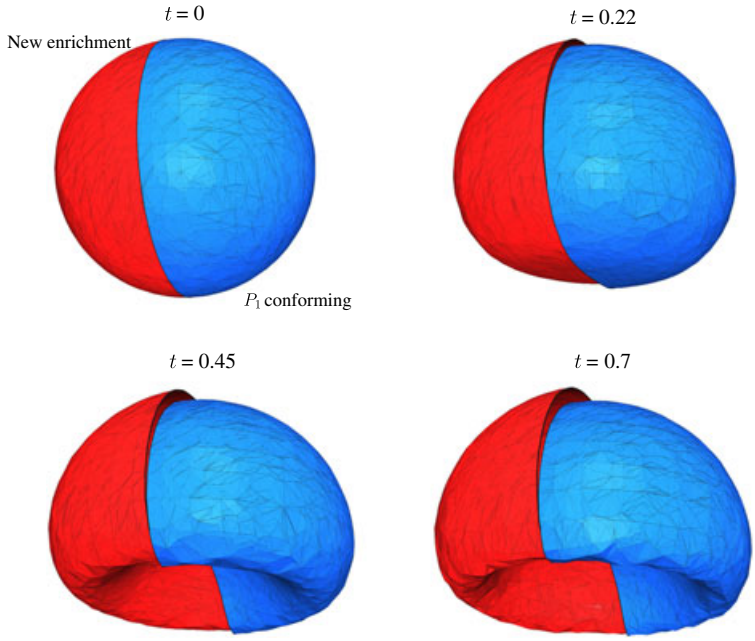

Figure 14. Comparison of the three-dimensional rising bubbles at different times for the skirted regime, using the new enrichment space (left, red) and the classical P_1-conforming space (right, blue).

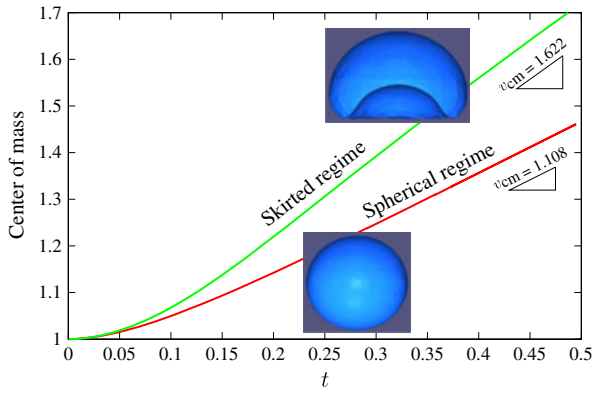

Figure 15. Bubble's center of mass as a function of time for the two regimes considered using the new enrichment space.

Table III. Physical parameters for the two regimes considered for the rise of a buoyant bubble in 3D.

Regime	Mo	We	Re_e	Re_c
Spherical	8.1×10^{-5}	1	5	3.93
Skirted	1	100	20	16.22

function of Codina–Coppola-Owen [44] (for kinks in the pressure field) and the new enrichment functions proposed in this paper leading to a triple enrichment. We illustrate the triple enrichment by means of two numerical examples. On the other hand, we propose without testing it, an enrichment of the velocity field to capture discontinuities in its gradient. Its evaluation is the subject of ongoing work.

DOI: 10.1002/fld

6.1. *Enrichment space of Codina–Coppola-Owen for kinks in the pressure field*

For completeness, we recall here the enrichment proposed in [44], which adds one shape function local to the elements crossed by the interface. This function can be easily defined with the help of a level set function ψ_h linearly interpolated on Ω_K and with the usual P_1 functions as follows

$$M_0(\mathbf{x}) = \frac{1}{2}\left(-|\psi_h(\mathbf{x})| + \sum_{J=1}^{n_p} |\psi_h(\mathbf{x}_J)| N_J(\mathbf{x})\right), \tag{41}$$

This function is defined as zero outside Ω_K and can thus be condensed before assembly. The enrichment function is illustrated for a typical triangular element in Figure 16, but the extension for the case of tetrahedral elements is straightforward as shown in Table IV where the code to calculate the shape function is included.

It is not difficult to see that the enrichment functions M_0, M_1 and M_2 are linearly dependent when the interface Γ_h becomes parallel to one of the element faces. Although this is very unlikely to happen during a general dynamical calculation, the linear independence of the finite element basis may be deteriorated if the interface becomes nearly parallel to one of the faces, resulting in a 3×3 matrix A_{MM} in Equation (27) approximately singular. This can be overcome by shifting the diagonal entries of A_{MM} by a small number when this situation is detected along a calculation,

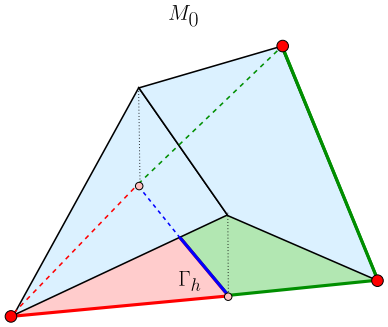

Figure 16. Codina–Coppola-Owen's enrichment function proposed in [44] in a typical triangular element.

Table IV. Computation of the enrichment function N_0^e for the space of [44]. Nomenclature: n_p is the number of nodes per element, n_G is the number of integration points per subelement, N_J is the usual Jth linear basis function, M_0 is the new enrichment function, $\boldsymbol{X}_J^K$ are the vertices coordinates of element Ω_K and ψ_h is the linearly interpolated level set function on Ω_K.

```
1: Subdivide element K in n_S subelements
2: do (s = 1, n_S)
3:   Set Gauss points x_j^s , for j = 1, ..., n_G
4:   do (i = 1, n_G)
5:     Set M_0(x_i^s) = 0
6:     if (ψ_h(x_i^s) > 0)
7:       Set M_0(x_i^s) = −ψ_h(x_i^s)
8:     end if
9:     do (J = 1, n_p)
10:      if (ψ_h(X_J^K) > 0) then
11:        Set M_0(x_i^s) ← M_0(x_i^s) + ψ_h(X_J^K) ∗ N_J(x_i^s)
12:      end if
13:    end do
14:  end do
15: end do
```


DOI: 10.1002/fld

that is,

$$\mathsf{A}_{MM} \leftarrow \mathsf{A}_{MM} + \varepsilon\, \mathsf{I}, \tag{42}$$

where I is the 3×3 identity matrix and ε is a small parameter that for the problems presented in this paper we choose as $10^{-4} \sum_{I,J} |A^{IJ}_{MM}|$.

6.2. Kinks and discontinuities in the pressure field

Two-fluid hydrostatic problem

The prototypical example in which there is a discontinuity in the pressure field and its gradient is the case of a two-fluid hydrostatic problem. We consider two fluids in a unit square domain with densities ρ_1 and ρ_2 and separated by the fixed interface $x_2 = a$ (the lighter fluid on the top of the other). At the interface, we introduce a singular force f_Γ of size 100 as shown in previous examples. The gravity g is taken equal to -10, the viscosity μ equal to 1 for both fluids, $\rho_1 = 100$, $\rho_2 = 1$ and $a = 0.5$. Non-slip boundary conditions are used at all walls. The exact solution for this problem consists in a velocity field identically zero and a pressure field given by

$$p(x_1, x_2) = \begin{cases} -\frac{1}{2}(\rho_1 + \rho_2)g + \rho_1\, g\, x_2 + f_\Gamma & \text{if } x_2 < \frac{1}{2} \\ \rho_2\, g(x_2 - 1) & \text{if } x_2 > \frac{1}{2} \end{cases} \tag{43}$$

Note that, there is a discontinuity in the pressure field of size f_Γ and a discontinuity in its gradient of size $(\rho_1 - \rho_2)|g| = 990$. In Table V, we show the $L^2(\Omega)$ and the $H^1(\Omega)$ error norms for the pressure and the velocity fields respectively, for two different meshes with characteristic sizes $h = 0.0275$ and $h = 0.006875$ (the second and fourth meshes of the sequence used in problem 4.2) and using different finite element spaces. We consider, on the one hand, the combination of the enrichment of Codina–Coppola-Owen with the new enrichment space and the combination of the enrichment of Codina–Coppola-Owen with the space of [35]. In the first case, the error is almost zero because the exact solution simply belongs to the finite element space. In the second and third cases, the approximation error is significantly bigger because the exact solution is not in the approximation space.

Extensional flow with discontinuous volume force

We finally consider the same problem shown in section 4.2 but in this case we introduce a discontinuous volume force as follows

$$\mathbf{b} = \begin{cases} -10\, \mathbf{e}_2 & \text{if } x_2 < a \\ 0 & \text{if } x_2 > a \end{cases} \tag{44}$$

As a result, the pressure field and its gradient are discontinuous, for which the triple enrichment used before becomes suitable. The pressure field for this problem is given by

$$p(x_1, x_2) = \rho \left(x_1 - \frac{1}{2}(x_1^2 + x_2^2) - |\mathbf{b}|\, x_2 \right) + 2(\mu_1 - \mu_2)\mathcal{H}(a - x_2) \tag{45}$$

in which there is a discontinuity of the pressure gradient of size $\rho\,|\mathbf{b}|$ and a discontinuity in the pressure of size $2\,(\mu_1 - \mu_2)$. In Table VI, we show the $L^2(\Omega)$-error norm for the pressure comparing the

Table V. Error norms of pressure and velocity on two different meshes for the two-fluid hydrostatic problem.

	$h = 0.0275$		$h = 0.006875$	
Pressure space	$\|\mathbf{u} - \mathbf{u}_h\|_{H^1(\Omega)}$	$\|p - p_h\|_{L^2(\Omega)}$	$\|\mathbf{u} - \mathbf{u}_h\|_{H^1(\Omega)}$	$\|p - p_h\|_{L^2(\Omega)}$
New space + [44]	10^{-13}	10^{-13}	10^{-13}	10^{-13}
New space alone	0.0206	0.1569	0.0023	0.0181
Space of [35] + [44]	0.1106	0.7574	0.0146	0.1018
P_1 space alone	8.0647	1.3995	3.9313	0.7456

DOI: 10.1002/fld

Table VI. $L^2(\Omega)$-error norm of the pressure as a function of the mesh size. Initial mesh with $h_0 = 0.056$.

Pressure space	h_0	$h_0/2$	$h_0/4$	$h_0/8$	$h_0/16$
New space + [44]	1.73×10^{-3}	5.84×10^{-4}	1.44×10^{-4}	3.56×10^{-5}	8.91×10^{-6}
New space alone	5.98×10^{-2}	2.35×10^{-2}	7.95×10^{-3}	2.83×10^{-3}	1.02×10^{-3}
Space of [35] + [44]	2.55×10^{-1}	8.97×10^{-2}	3.31×10^{-2}	1.21×10^{-2}	4.21×10^{-3}

use of the new enrichment and the space of [35], both combined with the enrichment of [44]. Also shown in the table is the case corresponding to the new enrichment alone. The pressure field being a quadratic function, the exact solution does not belong to the finite element space. From the table we observe that the order of convergence for the pressure field is proportional to h^2 in the first case and proportional to $h^{3/2}$ in the second one. Besides this difference, again the new enrichment space exhibits significantly smaller errors.

6.3. Kinks in the velocity field

Although it has not been tested yet, using the enrichment functions proposed by Codina–Coppola-Owen, a new enrichment of the velocity field to capture kinks in the velocity field, for problems involving Marangoni effects or two phase flows with $\mu_1/\mu_2 \gg 1$, can be devised. The idea in this case is to enrich each component of the velocity field as follows

$$u_i(\mathbf{x}) = \sum_{J \in \mathcal{J}} U_{iJ}\, N_J(\mathbf{x}) + c_i\, M_0(\mathbf{x}). \tag{46}$$

This new degree of freedom is not in $H^1(\Omega)$ and thus renders the approximation non-conforming. It could well happen that the errors introduced by this 'variational crime' are small, except perhaps in regions with high curvature for which local mesh refinement may be needed. The evaluation of this enrichment is still the subject of ongoing work.

7. CONCLUSIONS

A new enrichment space has been proposed to accommodate discontinuities in the pressure field for problems involving jumps at internal interfaces in multi-fluid flows. The new space consist of adding two degrees of freedom that are local to each element and can thus be condensed prior to assembly.

The new space has been tested and compared with other pressure spaces to accommodate discontinuities at immersed boundaries in several problems involving jumps in the pressure field and its gradient. In the classical Couette flow problem with a singular force the $L^2(\Omega)$ and $H^1(\Omega)$ error norms for pressure and velocity, respectively, exhibited practically the same results as using the space of [35]. For the extensional flow problem, the errors were much smaller (more than one order of magnitude) and with a better order of convergence for the new enrichment space as compared with the space of [35]. The new enrichment space has also been tested in a more challenging 3D problem involving a rising bubble in different regimes, exhibiting excellent results in terms of mass conservation as compared with the classical P_1-conforming space.

The possibility of combining the new enrichment with the enrichment proposed in [44] has also been explored in problems involving discontinuities and kinks in the pressure field because of the presence of singular forces and jumps in the density and/or in the volume forces. In this case, care has to be taken to avoid loss of the linear independence of the finite element basis, which can occur when the interface becomes parallel to one of the element faces.

The new proposed enrichment space is an attractive alternative to other existing finite element spaces to accommodate jumps at immersed boundaries.

DOI: 10.1002/fld

ACKNOWLEDGEMENTS

The authors acknowledge partial support from FAPESP and CNPq (Brazil) and from the ERC Advanced Grant "Real Time - Project AdG_2009325". The authors would also like to thank the International Center for Numerical Methods in Engineering for kindly supporting this work.

REFERENCES

1. Sommerfeld M, van Wachem B, Oliemans R. Special interest group on dispersed turbulent multi-phase flow, best practice guidelines. *ERCOFTAC*, 2007.
2. Hughes TJR, Liu WK, Zimmermann TK. Lagrangian–Eulerian finite element formulation for incompressible viscous flows. *Computer Methods in Applied Mechanics and Engineering* 1981; **29**:329–349.
3. Donea J, Huerta A, Ponthot J-P, Rodríguez Ferran A. *Arbitrary Lagrangian–Eulerian methods* (Stein E, de Borst R, Hughes T, eds), Encyclopedia of Computational Mechanics, Vol. 1. John Wiley & Sons: New York, 2004.
4. Hirt CW, Amsden AA, Cook JL. An arbitrary Lagrangian–Eulerian computing method for all flow speeds. *Journal of Computational Physics* 1974; **14**:227–253.
5. Cruchaga MA, Calentano DJ, Tezduyar TE. A moving Lagrangian interface technique for flow computations over fixed meshes. *Computer Methods in Applied Mechanics and Engineering* 2001; **191**:525–543.
6. Dettmer W, Saksono PH, Perić D. On a finite element formulation for incompressible Newtonian fluid flows on moving domains in the presence of surface tension. *Communications in Numerical Methods in Engineering* 2003; **19**:659–668.
7. Baiges J, Codina R, Coppola-Owen H. The fixed-mesh ALE approach for the numerical simulation of floating solids. *International Journal for Numerical Methods in Fluids* 2011; **67**(8):1004–1023. DOI: http://dx.doi.org/10.1002/fld.2403.
8. Idelsohn SR, Oñate E, Del Pin F. The particle finite element method: a powerful tool to solve incompressible flows with free-surfaces and breaking waves. *International Journal for Numerical Methods in Engineering* 2004; **61**:964–989.
9. Idelsohn SR, Mier-Torrecilla M, Oñate E. Multi-fluid flows with the particle finite element method. *Computer Methods in Applied Mechanics and Engineering* 2009; **198**:2750–2767.
10. Mier-Torrecilla M, Idelsohn SR, Oñate E. Advances in the simulation of multi-fluid flows with the particle finite element method. *International Journal for Numerical Methods in Fluids* 2010. DOI: http://dx.doi.org/10.1002/fld.2429. Published online.
11. Idelsohn SR, Mier-Torrecilla M, Nigro N, Oñate E. On the analysis of heterogeneous fluids with jumps in the viscosity using a discontinuous pressure field. *Computational Mechanics* 2010; **46**(1):115–124.
12. Unverdi S, Tryggvason G. A front-tracking method for viscous, incompressible, multi–fluid flows. *Journal of Computational Physics* 1992; **100**:25–37.
13. Gueyffier D, Lie J, Nadim A, Scardovelli R, Zaleski S. Volume-of-fluid interface tracking with smoothed surface stress methods for three-dimensional flows. *Journal of Computational Physics* 1999; **152**:423–456.
14. Popinet S, Zaleski S. A front-tracking algorithm for accurate representation of surface tension. *International Journal for Numerical Methods in Fluids* 1999; **30**:775–793.
15. Hirt CW, Nichols HD. Volume of fluid (VOF) methods for the dynamics of free boundaries. *Applied Numerical Mathematics* 1981; **39**:201–225.
16. Kothe DB, Rider WJ, Mosso SJ, Brock JS, Hochstein JI. Volume tracking of interfaces having surface tension in two and three dimensions. *Technical Report AIAA 96-0859*, AIAA, 1996. Presented at the 34rd Aerospace Sciences Meeting and Exhibit.
17. Cummins SJ, Francois MM, Kothe DB. Estimating curvature from volume fraction. *Computers and Structures* 2005; **83**:425–434.
18. Adalsteinsson D, Sethian J. A fast level set method for propagating interfaces. *Journal of Computational Physics* 1995; **118**:269–277.
19. Sethian JA. Evolution, implementation and application of level set and fast marching methods for advancing fronts. *Journal of Computational Physics* 2001; **169**:503–555.
20. Osher S, Fedkiw R. Level set methods: an overview and some recent results. *Journal of Computational Physics* 2001; **169**:463–502.
21. Guermond JL, Quartapelle L. A projection FEM for variable density incompressible flows. *Journal of Computational Physics* 2000; **165**:167–188.
22. Shu C, Osher S. Efficient implementation of essentially non-oscillatory shock-capturing schemes. *Journal of Computational Physics* 1988; **77**:439–471.
23. Jiang G-S, Peng D. Weighted ENO schemes for Hamilton–Jacobi equations. *SIAM Journal on Scientific Computing* 2000; **21**:2126–2144.
24. Sweby PK. High resolution schemes using flux limiters for hyperbolic conservation laws. *SIAM Journal on Numerical Analysis* 1984; **21**:995–1011.
25. Enright D, Fedkiw R, Ferziger J, Mitchell I. A hybrid particle level set method for improved interface capturing. *Computers and Structures* 2002; **83**:479–490.

26. Marchandise E, Remacle J-F, Chevaugeon N. A quadrature-free discontinuous Galerkin method for the level set equation. *Journal of Computational Physics* 2006; **212**:338–357.
27. Di Pietro D, Lo Forte S, Parolini N. Mass preserving finite element implementations of the level set method. *Applied Numerical Mathematics* 2006; **56**:1179–1195.
28. Enright D, Losasso F, Fedkiw R. A fast and accurate semi-Lagrangian particle level set method. *Computers and Structures* 2005; **83**:479–490.
29. Strain J. Semi Lagrangian methods for level set equations. *Journal of Computational Physics* 1999; **151**:498–533.
30. Strain J. Tree methods for moving interfaces. *Journal of Computational Physics* 1999; **151**:616–648.
31. Brackbill JU, Kothe DB, Zemach C. A continuum method for modeling surface tension. *Journal of Computational Physics* 1992; **100**:335–354.
32. Löhner R, Yang C, Oñate E. On the simulation of flows with violent free surface motion. *Computer Methods in Applied Mechanics and Engineering* 2006; **195**:5597–5620.
33. Carrica P, Wilson R, Stern F. An unsteady single-phase level set method for viscous free surface flows. *International Journal of Numerical Methods in Fluids* 2007; **53**:229–256.
34. Ganesan S, Matthies G, Tobiska L. On spurious velocities in incompressible flow problems with interfaces. *Computer Methods in Applied Mechanics and Engineering* 2007; **196**:1193–1202.
35. Ausas RF, Sousa FS, Buscaglia GC. An improved finite element space for discontinuous pressures. *Computer Methods in Applied Mechanics and Engineering* 2010; **199**:1019–1031.
36. Buscaglia G, Agouzal A. Interpolation estimate for a finite element space with embedded discontinuities. *IMA Journal of Numerical Analysis, accepted* 2011. DOI: 10.1093/imanum/drq045.
37. Minev PD, Chen T, Nandakumar K. A finite element technique for multifluid incompressible flow using Eulerian grids. *Journal of Computational Physics* 2003; **187**:255–273.
38. Chessa J, Belytschko T. An extended finite element method for two-phase fluids. *Journal of Applied Mechanics* 2003; **70**:10–17.
39. Belytschko T, Moës N, Usui S, Parimi C. Arbitrary discontinuities in finite elements. *International Journal for Numerical Methods in Engineering* 2001; **50**:993–1013.
40. Gross S, Reusken A. Finite element discretization error analysis of a surface tension force in two-phase incompressible flows. *SIAM Journal on Numerical Analysis* 2007; **45**:1679–1700.
41. Gross S, Reusken A. An extended pressure finite element space for two-phase incompressible flows with surface tension. *Journal of Computational Physics* 2007; **224**:40–58.
42. Reusken A. Analysis of an extended pressure finite element space for two-phase incompressible flows. *Computing and Visualization in Science* 2008; **11**:293–305.
43. Fries T-P, Belytschko T. The intrinsic XFEM: a method for arbitrary discontinuities without additional unknowns. *International Journal for Numerical Methods in Engineering* 2006; **68**:1358–1385.
44. Coppola-Owen AH, Codina R. Improving eulerian two-phase flow finite element approximation with discontinuous gradient pressure shape functions. *International Journal for Numerical Methods in Fluids* 2005; **49**:1287–1304.
45. Buscaglia GC, Ausas RF. Variational formulations for surface tension, capillarity and wetting. *Computer Methods in Applied Mechanics and Engineering* 2011; **200**(45-46):3011–3025.
46. Bänsch E. Finite element discretization of the Navier–Stokes equation with a free capillary surface. *Numerische Mathematik* 2001; **88**:203–235.
47. Codina R. A stabilized finite element method for generalized stationary incompressible flows. *Computer Methods in Applied Mechanics and Engineering* 2001; **190**:2681–2706.
48. Chang Y, Hou T, Merriman B, Osher S. A level set formulation of eulerian capturing methods for incompressible fluid flows. *Journal of Computational Physics* 1996; **124**:449–464.
49. Hughes T. Recent progress in the development and understanding of SUPG methods with special reference to the compressible Euler and Navier–Stokes equations. *International Journal for Numerical Methods in Fluids* 1987; **7**:1261–1275.
50. Marchandise E, Geuzaine P, Chevaugeon N, Remacle JF. A stabilized finite element method using a discontinuous level set approach for the computation of bubble dynamics. *Journal of Computational Physics* 2007; **225**:949–974.
51. Clift R, Grace J, Weber M. *Bubbles, Drops and Particles*. Dover publications: Mineola, New York, 2005.
52. Ausas R. Numerical simulation in two-phase immiscible flows with applications in hydrodynamic lubrication. *PhD Thesis*, Engineering, Instituto Balseiro, April, 2010.
53. Mut F, Buscaglia G, Dari E. New mass-conserving algorithm for level set redistancing on unstructured meshes. *Journal of Applied Mechanics* 2006; **73**:1011–1016.
54. Ausas RF, Buscaglia GC, Dari EA. A geometric mass-preserving redistancing scheme for the level set function. *International Journal for Numerical Methods in Fluids* 2011; **65**:989–1010.

DOI: 10.1002/fld